Table 3. Atomic Ratios of Phosphorus (P) vs Carbon (C) (P/C) of PMvN Measured by XPS at 15° and 90° of the Takeoff Angles of the Photoelectrons

	P/C	
sample	15°	90°
PMvN	0.034	0.040
PMB	0.024	0.030

of PMvN in the mixture of ethanol/water (volume fraction, 20/80) was 10.5 nm. These results suggest that PMvN formed an aggregate in the coating solvent, a mixture of ethanol/water (volume fraction, 20/80), and that the outer layer of the aggregate was covered with phosphorylcholine groups. The T_g of PMvN was 154 °C, which was moderately higher than that of PMB.[5] This indicates that at room temperature, the mobility of the polymer chains of PMvN is restricted. Figures 2 and 3 show the ^{1}H NMR and the FT-IR spectra of PMvN, respectively. In the NMR spectrum, there was a distinctive peak at 3.2 ppm of PMvN due to the $-N^+(CH_3)_3$ in the MPC and another characteristic broad peak at 6.7−8.1 ppm due to the $-C_{10}H_7$ of the vN moiety. In the FT-IR spectrum, prominent peaks were observed at 966, 1078, 1242, and 1718 cm^{-1} that indicate the presence of $-N^+(CH_3)_3$, P−O−C, O=P−O$^-$, and C=O, respectively. In addition, there were 3 peaks at 752, 821, and 858 cm^{-1} due to the adsorptions of β-displacement naphthalene.

3.2. Surface Characterization of PMvN on PET Plate. Surface elemental analysis of PMvN-coated PET plate was performed using XPS. As shown in Figure 4, the signals observed at 133 and 403 eV were attributed to phosphorus and nitrogen atoms in the MPC unit, respectively. The atomic ratios of phosphorus (P) vs carbon (C) (P/C) of PMvN and PMB measured by XPS at 15° and 90° of the takeoff angles of the photoelectrons were summarized in Table 3. The escape depths at 15° and 90° of the takeoff angles of the photoelectrons are approximately <2 nm and 5−10 nm, respectively. The P/C ratios of PMvN analyzed at 15° and 90° of the takeoff angles of the photoelectrons were much higher than those of PMB. Moreover, the P/C ratio of PMvN analyzed at 15° was greater than that of PMB analyzed at 90°. It has been reported that the P/C ratio of PMB analyzed for the photoelectrons takeoff angle of 15° becomes identical to that for 90° when PMB had been hydrated and freeze-dried prior to analysis.[11] These results suggest that the phosphorylcholine groups of PMvN are enriched on the extreme surface of the sample even under dry conditions. Figure 5 shows images of water droplets on the PET surface and the PMvN-coated and PMB-coated PET surfaces after 2 s of contact. On the noncoated PET plate and PMB-coated PET plate, the droplets almost formed a semicircle shape, i.e., the water contact angle was very large. On the other hand, the droplet on the PMvN-coated PET plate spread rapidly, indicating that the contact angle was extremely small. Coating with PMvN provided superior hydrophilicity without the wetting pretreatment. Figure 6 shows the DCA curves of the PMvN-coated and PMB-coated PET plates. Table 4 summarizes the values of θ_A and θ_R obtained from Figure 6. As shown in Table 4, the PMB-coated PET plate had large hysteresis (Figure 6) corresponding to a large θ_A and a small θ_R. Under dry conditions, the phosphorylcholine groups of PMB were covered with the hydrophobic polymer chains; this induced a decrease in the surface free energy.[11] On the other hand, the phosphorylcholine groups should be exposed to the aqueous environment in order to reduce the interfacial free energy. Thus, the observed large hysteresis for PMB may be related to the reorientation of the phosphorylcholine groups. In this method, a long pretreatment time is required for the phosphorylcholine groups to achieve equilibrium. Therefore, if the PET plate was coated with PMB, the surface of the plate did not show good blood compatibility without the wetting pretreatment prior to contact with blood.[11] On the other hand, no hysteresis was observed in the DCA curve of the PMvN-coated PET plate. Moreover, its values of both θ_A and θ_R were small. This may be attributed to the ability of the PMvN network to enrich the phosphorylcholine groups at the surface and immobilize them even under dry conditions. On the basis of the Mf value, the mobility of the polymer chains in PMvN was expected to be quite low due to the high T_g of PMvN. Figure 7 shows the expected surface structure of PMvN under dry conditions. We suggest that the process of development of this surface structure is as follows. PMvN in the mixed coating solvent of ethanol/water (volume fraction, 20/80) results in the formation of aggregates, and the outer layers of the aggregates are covered with phosphorylcholine groups. Subsequently, during solvent evaporation, the surface orientation of the phosphorylcholine groups is strictly immobilized due to the rather low mobility of PMvN. Therefore, as shown in Figure 7, even under the dry conditions, the PMvN coating provides a surface enriched with phosphorylcholine groups.

Table 4. Advancing and Receding Contact Angles of Water Applied under the Dry Condition (PET plate)

	contact angle (deg)		
sample	advancing	receding	MF[a]
PMvN	24	22	0.083
PMB	101	16	0.84
noncoating	90	60	0.33

[a] Mobility factor.

3.3. Protein Adsorption under Dry Conditions. Figure 8 shows the amount of BSA adsorbed on the PET plates coated with the MPC polymers. The PMB-coated PET surface was not in equilibrium with phosphorylcholine groups because the incubation time was merely 60 min. It is reported that the PMB coating requires 300 min of wetting to reach equilibrium hydration by reorientation of the phosphorylcholine groups.[11] On the PET surface, BSA adsorption was significant. When BSA solution was in contact with the PET plate coated with MPC polymers under dry conditions without the wetting pretreatment, the amount

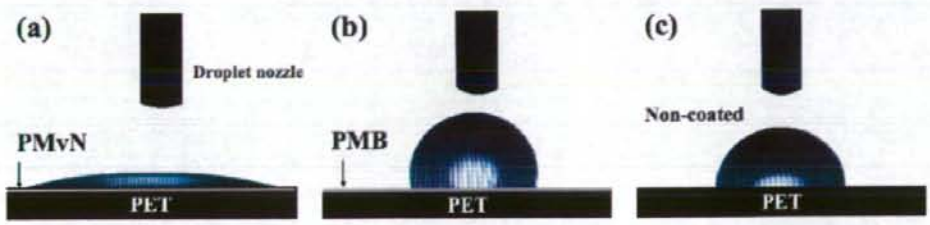

Figure 5. Water droplets on the surfaces under dry condition after contact for 2 s: (a) PMvN-coated PET, (b) PMB-coated PET, (c) noncoated PET.

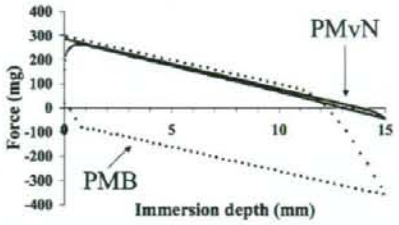

Figure 6. DCA curves of the PMvN-coated and PMB-coated PET plates dipped in water at a speed of 80 μm/s. The curve of the PMvN-coated PET plate shows an extremely hydrophilic and motionless surface.

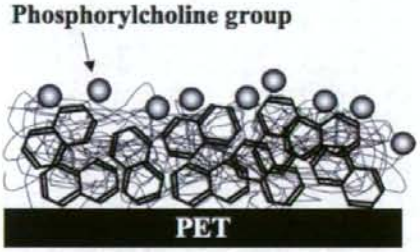

Figure 7. Expected surface structure of PMvN on the PET surfaces under dry conditions. The phosphorylcholine groups are enriched on the surface even in the dry condition.

of adsorbed BSA reduced significantly compared with the amount that was adsorbed on the PET plates. However, more effective protein adsorption resistance was observed with the PMvN coating. This difference between the two MPC polymers may be their state of hydration due to the density and orientation of the phosphorylcholine groups in the polymer. The amount of BSA adsorption to achieve equilibrium on the PMB-coated PET

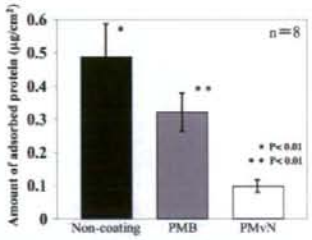

Figure 8. The amount of adsorbed BSA on the polymer surfaces under dry conditions. The sample plates were in contact with 0.45 g/dL BSA solution for 60 min at 37 °C.

plate after pretreatment was 0.12−0.30 μg/cm^2.[24] This implies that the PMvN-coated surface was the same as this equilibrated surface. Thus, we could develop an MPC polymer surface that provided rapid hydrophilicity and protein adsorption resistance when in contact with protein solutions even under dry conditions.

4. Conclusion

PMvN is capable of forming a phosphorylcholine group-enriched surface from its solution during the polymer-coating process. Under dry conditions, these surfaces immediately showed hydrophilicity and protein-adsorption resistance on contact with protein solutions. Therefore, PMvN may have a potential application as a coating polymer in blood-contacting medical devices, which require excellent blood compatibility.

Acknowledgment. A part of this research was supported by the Core Research for Evolution Science and Technology (CREST), Japan Science and Technology Agency.

LA801017H

(24) Ishihara, K.; Nomura, H.; Mihara, T.; Kurita, K.; Iwasaki, Y.; Nakabayashi, N. *J. Biomed. Mater. Res.* **1998**, *39*, 323.

Applied Surface Science 255 (2008) 379–383

Contents lists available at ScienceDirect

Applied Surface Science

journal homepage: www.elsevier.com/locate/apsusc

Protein adsorption resistant surface on polymer composite based on 2D- and 3D-controlled grafting of phospholipid moieties

Toru Hoshi [a], Ryosuke Matsuno [a,c], Takashi Sawaguchi [d], Tomohiro Konno [a,c], Madoka Takai [a,c], Kazuhiko Ishihara [a,b,c,*]

[a] Department of Materials Engineering, School of Engineering, The University of Tokyo, 7-3-1 Hongo, Bunkyo-ku, Tokyo 113-8656, Japan
[b] Department of Bioengineering, School of Engineering, The University of Tokyo, 7-3-1 Hongo, Bunkyo-ku, Tokyo 113-8656, Japan
[c] Center for NanoBio Integration, The University of Tokyo, 7-3-1 Hongo, Bunkyo-ku, Tokyo 113-8656, Japan
[d] Department of Materials and Applied Chemistry, College of Science and Technology, Nihon University, 1-8-14 Kanda-surugadai, Chiyoda-ku, Tokyo 101-8308, Japan

ARTICLE INFO

Article history:
Available online 1 July 2008

PACS:
68.47.Mn
82.35.−x
81.05.Lg

Keywords:
2-Methacryloyloxyethyl phosphorylcholine polymer
Polymer composite
Atom transfer radical polymerization
Surface modification

ABSTRACT

To prepare the biocompatible surface, a phosphorylcholine (PC) group was introduced on this hydroxyl group generated by surface hydrolysis on the polymer composite composed of polyethylene (PE) and poly (vinyl acetate) (PVAc) prepared by supercritical carbon dioxide. Two different procedures such as two-dimensional (2D) modification and three-dimensional (3D) modification were applied to obtain the steady biocompatible surface. 2D modification was that PC groups were directly anchored on the surface of the polymer composite. 3D modification was that phospholipid polymer was grafted from the surface of the polymer composite by surface-initiated atom transfer radical polymerization (SI-ATRP) of 2-methacryloyloxyethyl phosphorylcholine (MPC). The surfaces were characterized by X-ray photoelectron spectroscopy, dynamic water contact angle measurements, and atomic force microscope. The effects of the poly(MPC) chain length on the protein adsorption resistivity were investigated. The protein adsorption on the polymer composite surface with PC groups modified by 2D or 3D modification was significantly reduced as compared with that on the unmodified PE. Further, the amount of protein adsorbed on the 3D modified surface that is poly(MPC)-grafted surface decreased with an increase in the chain length of the poly(MPC). The surface with an arbitrary structure and the characteristic can be constructed by using 2D and 3D modification. We conclude that the polymer composites of PE/PVAc with PC groups on the surface are useful for fabricating biomedical devices due to their good mechanical and surface properties.

1. Introduction

The adsorption of proteins on the surface is recognized as the first event in determining subsequent biological events, including thrombus formation, foreign body reaction, bacterial infection, and other undesirable bioresponses [1]. Thus, there is considerable interest in surfaces that might inhibit or reduce protein adsorption [2]. One of the approaches to prepare a "protein resistant" surface is the incorporation of the phosphorylcholine (PC) group that is a phospholipid polar group of a major component of the outer membrane of cells. Ishihara et al. synthesized one of the PC group-bearing monomers, 2-methacryloyloxyethyl phosphorylcholine (MPC) [3]. Since MPC-based polymers provide resistance to protein adsorption and cell adhesion, they use the surface of blood-contacting and implantable medical devices [4–15].

For preparing well-defined surface, surface-initiated atom transfer radical polymerization (SI-ATRP) is particularly useful because of its versatility with respect to the monomer type, its tolerance of impurities, and the typically mild reaction conditions under which it is conducted [16]. Feng et al. and Iwata et al. reported the graft polymerization of MPC by SI-ATRP from silicon surfaces that were functionalized with 2-bromoisobutyl derivatives [17–19]. The surface showed excellent protein adsorption resistance when the polymer chain length and density were optimized. The grafting of poly(MPC) instead of silicone on the surface of a soft polymer material is considerably useful for developing new biomaterials and biomedical devices.

Recently, we succeeded in the preparation of a polymer composite composed of polyethylene (PE) and poly (vinyl

* Corresponding author at: Department of Materials Engineering, School of Engineering, The University of Tokyo, 7-3-1 Hongo, Bunkyo-ku, Tokyo 113-8656, Japan.
E-mail address: ishihara@mpc.t.u-tokyo.ac.jp (K. Ishihara).

0169-4332/$ – see front matter © 2008 Elsevier B.V. All rights reserved.
doi:10.1016/j.apsusc.2008.06.145

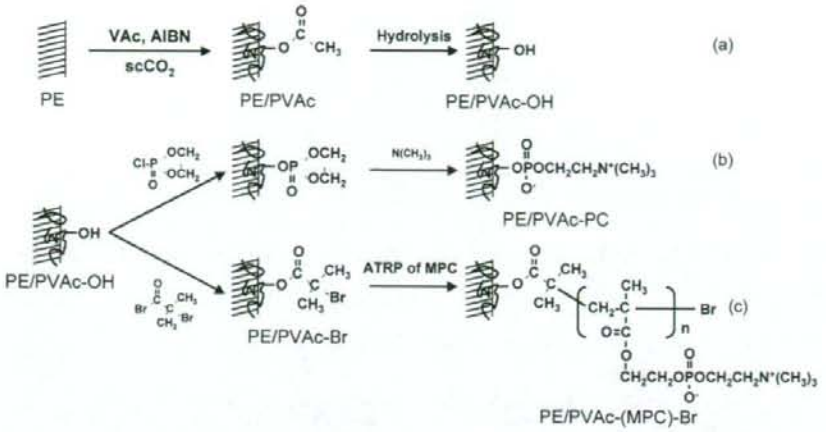

Fig. 1. Synthetic route of poly(MPC)-grafted polymer composite through SI-ATRP.

acetate) (PVAc) by *in situ* polymerization of vinyl acetate in the PE substrate by using supercritical carbon dioxide ($scCO_2$) fluid [20,21]. Further, we converted the acetyl groups in PVAc on the surface of the polymer composite to hydroxyl groups following the PC groups (Fig. 1(a) and (b)). In this way, the surface prepared by two-dimensional (2D) correction in which the PC group was anchored directly on the surface of the polymer composite suppressed effectively the protein adsorption. It is expected that new polymer biomaterials could be created by the new method that is the surface modification of polymer composite prepared by $scCO_2$.

In this study, the biocompatible surface was constructed by three-dimensional (3D) modification, that is, the phospholipid polymer was grafted from the surface of the polymer composite by SI-ATRP of MPC. The surface initiator was immobilized by the reaction between 2-bromoisobutyryl bromide and the hydroxyl group on the polymer composite surface. Subsequently, graft polymerization of MPC was carried out by the SI-ATRP method (Fig. 1(c)). We reported the 3D-controlled poly(MPC)-grafted surface on the PE/PVAc polymer composite. Further, we discussed that the effect of the poly(MPC) chain length on the surface properties and protein adsorption behavior compared with those of PC group directly immobilized surface.

2. Experiment

2.1. Materials

PE/PVAc, PE/PVAc-OH, and PE/PVAc-PC were synthesized and purified by a method reported previously [20,21], as shown in Fig. 1(a) and (b). 2-Bromoisobutyryl bromide, 2,2′-bipyridyl (Bpy), ethyl-2-bromoisobutyrate, copper(I) bromide (CuBr), and fluorescein isothiocyanate-labeled bovine serum albumin (FITC–BSA) were purchased from Sigma–Aldrich Co., Saint Louis, USA, and used as-received. The other reagents were purified by conventional distillation.

2.2. Preparation of poly(MPC)-grafted polymer composite: PE/PVAc-(MPC)-Br

On the surface of PE/PVAc-OH, 2-bromoisobutyryl bromide was reacted to introduce the initiator of SI-ATRP (PE/PVAc-Br). Argon gas was purged in methanol to eliminate oxygen before the polymerization. MPC (0.01 mol) was added to the Schlenk flask containing a magnetic stir bar and was subsequently dissolved in 10 mL of methanol bubbled with argon for 15 min to eliminate oxygen. CuBr and Bpy were added to the MPC solution with stirring under argon. After being stirred for 30 min under an argon gas atmosphere, the PE/PVAc-Br plate was submerged to the flask. Ethyl-2-bromoisobutyrate was then added as a sacrificial initiator ([I]). The graft polymerization was performed at 25 °C with stirring under an argon gas atmosphere. After 24 h, the poly(MPC)-grafted polymer composite (PE/PVAc-(MPC)-Br) plate was removed from the polymerization mixture and rinsed with methanol and water. Subsequently, the PE/PVAc-(MPC)-Br plate was dried *in vacuo* at room temperature after being extracted with methanol for 24 h to remove the unreacted reagents and homopolymer by using a Soxhlet-extractor. Four different [MPC]/[I] ratios, 50, 100, 150, and 200, were applied to prepare poly(MPC)-grafted polymer composites with different poly(MPC) chain lengths (MPC monomer units). The polymerization condition is as follows: [MPC] = 1.0 M, [CuBr]:[Bpy]:[I] = 1:2:1.

The molecular weight of free poly(MPC) in solution was measured by gel permeation chromatography (GPC) using a Shodex SB-804HQ column (upper limit of the molecular weight was $\sim 1.0 \times 10^7$ g/mol, the flow rate was 0.40 mL/min).

Surface characterizations of the sample were carried out by X-ray photoelectron spectroscopy (XPS) (AXIS-HSi, Shimadzu/KRATOS, Kyoto, Japan), dynamic water contact angle (DCA) measurement (CA-W, Kyowa Interface Science Co., Tokyo, Japan), and atomic force microscopy (AFM) (NanoScope IIIa Multimode SPM, Veeco Instruments, Tokyo, Japan).

2.3. Protein adsorption test

Polymer composites with poly(MPC)-grafted surface were exposed to 4.5 mg/mL FTIC-BSA in Dulbecco's phosphate-buffered saline (PBS) at 37 °C for 60 min and then rinsed five times with fresh PBS. The FITC–BSA concentration was 10% of the plasma concentration. The sample was dried in an argon stream and observed with a fluorescence microscope. The relative fluorescent intensity based on the adsorbed protein on the surface was calculated by comparison with the adsorbed protein on the unmodified PE surface.

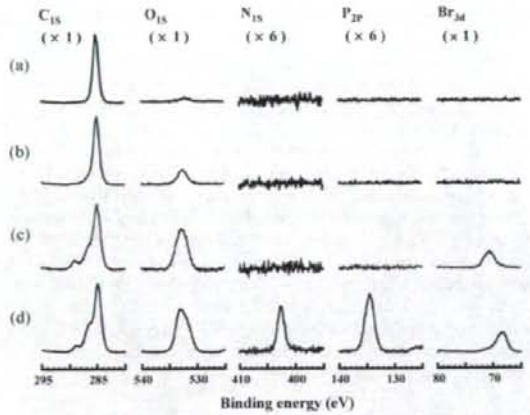

Fig. 2. XPS charts of (a) unmodified PE, (b) PE/PVAc-OH, (c) PE/PVAc-Br, and (d) PE/PVAc-(MPC)-Br ([MPC]/[I] = 100). The intensities of each atom were normalized by the intensity of C 1s at 285 eV.

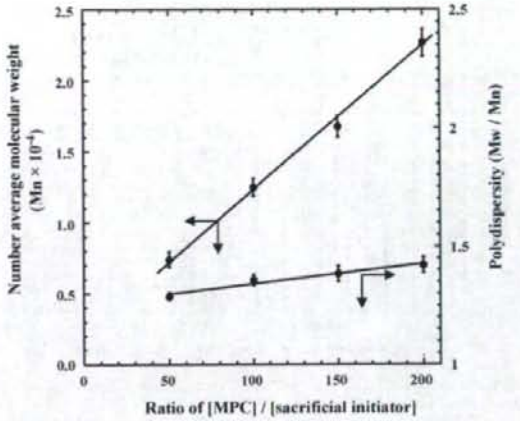

Fig. 3. Relationship between [MPC]/[sacrificial initiator] values and molecular weight of the poly(MPC) formed.

3. Results and discussion

3.1. Preparation of poly(MPC)-grafted polymer composite

Fig. 2 shows the XPS charts of unmodified PE, PE/PVAc-OH, PE/PVAc-Br and PE/PVAc-(MPC)-Br. In the unmodified PE, a strong intensity was observed at 285 eV (Fig. 2(a)). This is attributed to the carbon atoms in the methylene chain. The XPS peaks of PE/PVAc-OH broadened in the C 1s region and new peaks corresponding to the hydroxyl group were observed in the O 1s region (Fig. 2(b)). After the immobilization of the ATRP initiator on the polymer composite (Fig. 2(c)), the XPS peaks became broad in the C 1s region, the peak intensity of the O 1s region increased and the new peak was observed in the Br 3d region. This broad peak was attributed to the 2-bromoisobutyl groups in the C 1s region. An increase in the intensity of the O 1s region and the new peak in the Br 3d region were attributed to the carbonyl group (C=O) and bromine on the 2-bromoisobutyl groups, respectively. After the grafting of poly(MPC) (Fig. 2(d)), the increase in the peak intensity is caused by the increase in the amount of oxygen in the O 1s region, moreover, the nitrogen and phosphorus peaks were observed at 403 eV and 134 eV, respectively, and these peaks were attributed to the PC groups. In addition, the position of the bromine peak was shifted from a binding energy of 71–69 eV by the SI-ATRP of MPC monomer. These results confirmed that the surface initiator for the SI-ATRP was immobilized on the PE/PVAc polymer composite and the SI-ATRP of MPC succeeded had been successfully performed.

In this study, we added ethyl-2-bromoisobutyrate ([I]) as the sacrificial initiator to the polymerization solution to provide a deactivator that was concentration sufficiently high for the control of ATRP grafting from the surface of PE/PVAc-Br. The added sacrificial initiator also facilitated the control of the polymer chain length through the variation of the [MPC]/[I] ratio, assuming that the chains grown from the surface and in solution have similar molecular weights. This assumption was proved to be valid for the PMMA-grafted PE films [22]. Figs. 3 and 4 show the relationship between the molecular weight of poly(MPC) and the atomic surface composition with the [MPC]/[I] ratio, respectively. The number average of the molecular weight (Mn) of poly(MPC) and the phosphorus composition (P 2p/C 1s ratio determined by XPS) increased linearly with the [MPC]/[I] ratio, suggesting that the

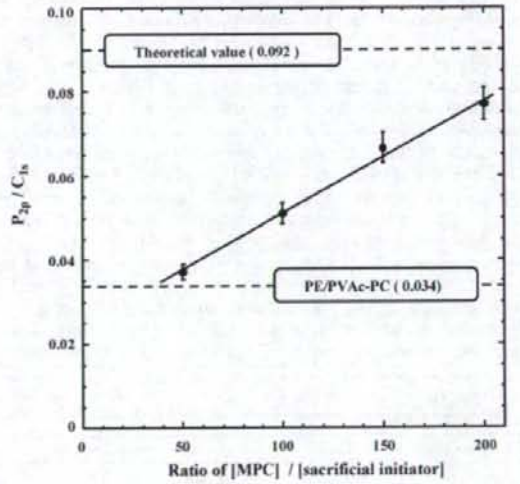

Fig. 4. Relationship between [MPC]/[sacrificial initiator] values and P 2p/C 1s values determined by XPS analysis.

ATRP grafting of MPC from the polymer composite surface was well-controlled process. In addition, the value of the P 2p/C 1s ratio approaches the theoretical value (0.092) as the chain length of poly(MPC) increases. This fact indicates that the density of the PC group on the surface increases with the chain length of the grafted poly(MPC). Further, the value of the P 2p/C 1s ratio of PE/PVAc-PC (0.034) was almost the same in the case of small graft chain lengths ([MPC]/[I] = 50). In this case, it is thought that the poly(MPC)-grafted surface ([MPC]/[I] = 50) and PE/PVAc-PC have similar surface properties.

3.2. Contact angle measurements

Dynamic water contact angle measurement has commonly been used to characterize the relative hydrophilicity or hydrophobicity of surfaces [23]. For surfaces with comparable structures, a relatively low contact angle value generally implies high

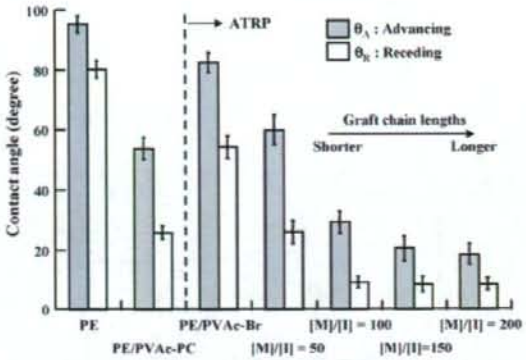

Fig. 5. Advancing and receding water contact angles of poly(MPC)-grafted surfaces of the polymer composite.

hydrophilicity. Fig. 5 shows the results of the DCA measurements. The advancing (θ_A) and receding (θ_R) contact angles decreased with the introduction of PC groups on the surface. Moreover, the poly(MPC)-grafted surface ([MPC]/[I] = 50) and PE/PVAc-PC with almost the same surface composition exhibited similar hydrophilicity. In the case of large graft-chain lengths, the hydrophilicity of the surface increased considerably. PE/PVAc-OH caused a hydrophilic/hydrophobic microphase separation because the surface of PE/PVAc assumed a microdomain structure comprising of crystalline of PE and amorphous regions (PE and PVAc amorphous) [21]. The surface initiator could be introduced only in hydroxyl groups generated in the hydrophilic domain based on the PVAc, and MPC could be polymerized from the domain by introducing the surface initiator. Therefore, the short poly(MPC)-grafted chains did not cover the hydrophobic domain based on PE; however, the long graft chains could cover the hydrophobic domain. Thus, the hydrophilicity of the polymer composite surfaces was greatly improved by the introduction of the poly(MPC) graft. Consequently, we inferred that the surface density of the PC groups considerably influences the surface properties and 3D modification is preferred to 2D modification, which is achieved by the direct immobilization of PC groups.

3.3. Surface morphology

The wet condition topology of the surfaces was examined by employing fluid tapping mode AFM in pure water. Fig. 6 shows height images of the unmodified PE and grafted poly(MPC) surfaces. The unmodified PE surface was smooth with a root mean square (RMS) roughness of 1.60 nm. The surface of the introduced surface initiator had an RMS roughness of 4.78 nm (Fig. 6(d)–(f)) indicate that the morphology of poly(MPC)-grafted surface was dependent on the poly(MPC) chain length. The surface containing chains with small lengths showed a greater roughness (Fig. 6(e)) as compared to the surfaces comprising chains with large lengths (Fig. 6(f)), as is evident from the RMS data. Further, on the surface of longer chain length ([MPC]/[I] = 100), regular peaks and valleys were observed within the measurement areas. These results indicated that the surface was covered with long poly(MPC)-graft chains.

3.4. Protein adsorption test

Fig. 7 shows the fluorescent intensity of the FITC–BSA adsorbed on the surfaces. The fluorescent intensity is proportional to the amount of adsorbed protein on the surface. The amount of the FITC–BSA adsorbed on the surface was in good agreement with the contact angle with water depended on the density of the PC groups, as shown in Fig. 5. The PC group immobilized surface effectively reduced protein adsorption as compared with unmodified PE; further, the amount of protein adsorbed on the poly(MPC)-grafted surface decreased with an increase in the chain length of poly(MPC). Both the hydrophilicity and surface morphology are significant factors for the protein adsorption resistance properties. The suppression of protein adsorption by the poly(MPC)-grafted surface was considerably greater than that on PE/PVAc-PC because of the higher density of PC groups. The amount of protein adsorbed on the poly(MPC)-grafted surface decreased with an increase in the chain length of grafted poly(MPC). We determined the amount of adsorbed BSA on the unmodified PE and PE/PVAc-PC surface quantitatively and it was 1.12 $\mu g/cm^2$ and 0.22 $\mu g/cm^2$, respectively [20]. The value obtained on the PC group immobilized surface was sufficient to suppress thrombus formation even when the surface was in contact with blood [24]. Thus, such significant reduction in protein adsorption that was observed in the case of

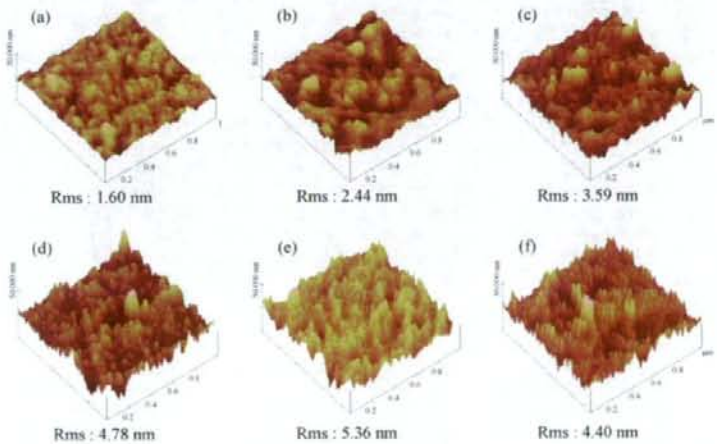

Fig. 6. AFM 3D height images of (a) unmodified PE, (b) PE/PVAc-OH, (c) PE/PVAc-PC, (d) PE/PVAc-Br, (e) PE/PVAc-(MPC)-Br ([MPC]/[I] = 50), and (f) PE/PVAc-(MPC)-Br ([MPC]/[I] = 100) (image size: 1 μm × 1 μm × 50 μm).

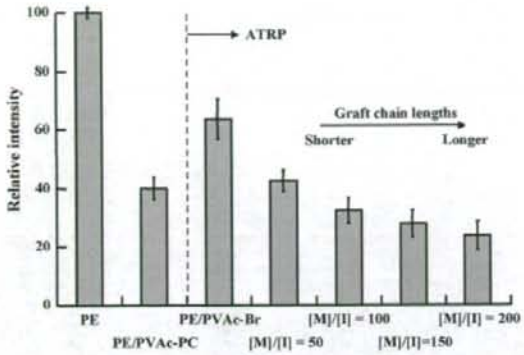

Fig. 7. Relative fluorescence intensity based on the FITC–BSA adsorbed on the various surfaces.

the poly(MPC)-grafted surface may be good for the inhibition of thrombus formation. Therefore, the 3D regulated aliment of PC groups on the surface of the polymer composite has excellent potential in the fabrication of biomedical devices.

4. Conclusion

The surface modification of polyolefins such as PE is very difficult because of these low surface tension and chemical stability. If the grafts are covalently attached to the substrate, the modified layer is stable and does not delaminate. To prepare for the biocompatible surface, phospholipid moieties were directly anchored on the new polymer composite with hydroxyl groups on the surface through the surface reaction of hydroxyl groups. Two different procedures such as 2D modification and 3D modification were applied to obtain the steady biocompatible surface. Our previous article demonstrated the 2D modification that PC groups were directly anchored on the surface of the polymer composite. In this study, we have reported a versatile approach that is 3D modification for preparing poly(MPC)-grafted substrates based on a novel synthetic method of polymer composites and SI-ATRP. 3D modification was that phospholipid polymer were grafted from the surface of the polymer composite by SI-ATRP of MPC. By varying the [MPC]/[sacrificial initiator] ratio, a set of surfaces corresponding to various graft chain lengths was prepared. The density of the PC groups on the surface, which are closely related to the hydrophilicity, increased with the length of the grafted poly(MPC) chains. The surfaces with high poly(MPC) chain lengths showed a drastic reduction in protein adsorption. The surface with an arbitrary structure and the characteristic can be constructed by using 2D and 3D modification. In addition, another monomer enables to polymerize from the terminal halogen group of graft MPC polymer chain using SI-ATRP. The various functional biointerface is constructed by the choice of next monomer with the functional groups such as carboxylic acid, amine, active ester, epoxy, and cell adhesion molecule. We conclude that the present process for preparing protein adsorption resistant surfaces on polymer composites by the SI-ATRP of MPC will provide an excellent method for developing new biomedical devices.

References

[1] Proteins at interfaces II, fundamentals and applications, T.A. Horbett, J.L. Brash (Eds.), ACS Symposium Series No. 602, ACS, Washington, DC, 1995.
[2] J.L. Brash, J. Biomater. Sci. Polym. Ed. 11 (2000) 1135.
[3] K. Ishihara, T. Ueda, N. Nakabayashi, Polym. J. 22 (1990) 355.
[4] T. Ueda, H. Oshida, K. Kurita, K. Ishihara, N. Nakabayashi, Polym. J. 24 (1992) 1259.
[5] K. Ishihara, R. Aragaki, T. Ueda, A. Watanabe, N. Nakabayashi, J. Biomed. Mater. Res. 24 (1990) 1069.
[6] K. Ishihara, N.P. Ziats, B.P. Tierney, N. Nakabayashi, J.M. Anderson, J. Biomed. Mater. Res. 25 (1991) 1397.
[7] K. Ishihara, H. Oshida, T. Ueda, Y. Endo, A. Watanabe, N. Nakabayashi, J. Biomed. Mater. Res. 26 (1992) 1543.
[8] K. Ishihara, H. Nomura, T. Mihara, K. Kurita, Y. Iwasaki, N. Nakabayashi, J. Biomed. Mater. Res. 39 (1998) 323.
[9] A. Yamasaki, Y. Imamura, K. Kurita, Y. Iwasaki, N. Nakabayashi, K. Ishihara, Colloid Surf. B: Biointerfaces 28 (2003) 53.
[10] S. Sawada, S. Sakaki, Y. Iwasaki, N. Nakabayashi, K. Ishihara, J. Biomed. Mater. Res. 64A (2003) 411.
[11] K. Ishihara, D. Nishiuchi, J. Watanabe, Y. Iwasaki, Biomaterials 25 (2004) 1115.
[12] N. Morimoto, A. Watanabe, Y. Iwasaki, K. Akiyoshi, K. Ishihara, Biomaterials 25 (2004) 5353.
[13] S.H. Ye, J. i Watanabe, K. Ishihara, J. Biomater. Sci. Polym. Ed. 15 (2004) 981.
[14] T. Moro, Y. Takatori, K. Ishihara, T. Konno, Y. Takigawa, T. Matsushita, U.I. Chung, K. Nakamura, H. Kawaguchi, Nat. Mater. 3 (2004) 829.
[15] T. Goda, T. Konno, M. Takai, T. Moro, K. Ishihara, Biomaterials 27 (2006) 5151.
[16] J.B. Kim, W.X. Huang, M.D. Miller, G. Baker, M.L. Bruening, Polym J. Sci. Part A: Polym. Chem. 41 (2003) 386.
[17] W. Feng, S. Zhu, K. Ishihara, J.L. Brash, Langmuir 21 (2005) 5980.
[18] W. Feng, S. Zhu, K. Ishihara, J.L. Brash, Biointerphases 1 (2006) 50.
[19] R. Iwata, P.S. In, V.P. Hoven, A. Takahara, K. Akiyoshi, Y. Iwasaki, Biomacromolecules 5 (2004) 2308.
[20] T. Hoshi, T. Swaguchi, T. Konno, M. Takai, K. Ishihara, Polymer 48 (2007) 1573.
[21] T. Hoshi, T. Swaguchi, R. Matsuno, T. Konno, M. Takai, K. Ishihara, J. Supercrit. Fluids 44 (2008) 391.
[22] K. Yamamoto, Y. Miwa, H. Tanaka, M. Sakaguchi, S. Shimada, J. Polym. Sci. A: Polym. Chem. 40 (2002) 3350.
[23] T. Teraya, A. Takahara, T. Kajiyama, Polymer 31 (1990) 1149.
[24] K. Ishihara, Sci. Technol. Adv. Mater. 1 (2000) 131.

Colloids and Surfaces B: Biointerfaces 67 (2008) 216–223

Contents lists available at ScienceDirect

Colloids and Surfaces B: Biointerfaces

journal homepage: www.elsevier.com/locate/colsurfb

Surface immobilization of biocompatible phospholipid polymer multilayered hydrogel on titanium alloy

Jiyeon Choi[a], Tomohiro Konno[a,c], Ryosuke Matsuno[a,c], Madoka Takai[a,c], Kazuhiko Ishihara[a,b,c,*]

[a] Department of Materials Engineering, School of Engineering, The University of Tokyo, 7-3-1, Hongo, Bunkyo-ku, Tokyo 113-8656, Japan
[b] Department of Bioengineering, School of Engineering, The University of Tokyo, 7-3-1, Hongo, Bunkyo-ku, Tokyo 113-8656, Japan
[c] Center for NanoBio Integration, The University of Tokyo, 7-3-1, Hongo, Bunkyo-ku, Tokyo 113-8656, Japan

ARTICLE INFO

Article history:
Received 21 May 2008
Received in revised form 19 August 2008
Accepted 21 August 2008
Available online 16 September 2008

Keywords:
Phospholipid polymer
Hydrogel
Multilayer
Titanium
Biocompatibility

ABSTRACT

The aim of this study is to improve the biocompatibility of titanium alloy (Ti) implants by immobilization of multilayered phospholipid polymer hydrogel able to reduce protein adsorption and cell adhesion. We fabricated and characterized a multilayered hydrogel on Ti substrate via a layer-by-layer self-assembly deposition method using a phospholipid polymer bearing a phenylboronic acid moiety and poly(vinyl alcohol) (PVA). The water-soluble phospholipid polymer (PMBV) was synthesized from 2-methacrylocyloxyethyl phosphorylcholine, *n*-butyl methacrylate, and 4-vinylphenylboronic acid (VPBA). The PMBV reacted with PVA and formed a hydrogel due to covalent linkage between the VPBA units and hydroxyl groups of PVA. The hydrogel layer growth on the Ti surface was initialized by the deposition of one layer of photoreactive PVA bonded by UV irradiation to the Ti surface, which was modified with an alkylsilane compound. The multilayered hydrogel was built up by alternating the deposition of the PMBV and PVA; this was monitored by several methods: static contact angle measurement, X-ray photoelectron spectroscopy, and attenuated Fourier-transform infrared spectroscopy. The results revealed clearly the progressive construction of the multilayered hydrogel on the Ti substrate. The PMBV/PVA multilayer prepared on the Ti substrate reduced the adhesion of L929 cells compared with that on an untreated Ti substrate. Thus, we concluded that the formation of the multilayered hydrogel is effective to improve the biocompatibility on Ti-based medical devices.

1. Introduction

When medical implants come into contact with the biological environment, various biological responses ranging from the adsorption of biomolecules to cell attachment and tissue response should occur [1]. The design of biomedical devices for controlling the physical, chemical and biochemical properties of an implant surface is important since the unfavorable interaction at the interface between an implant and biological environment might lead to implant failure, complications with high morbidity and treatment costs [2,3]. Among the various biomaterials used for load-bearing applications, such as orthopedic and cardiovascular implants, titanium and its alloys (Ti) is the key material owing to its excellent tissue compatibility and corrosion resistance that stems from the native oxide layer. This oxide layer sometimes is beneficial to the adsorption of many proteins for healing process. However, in blood-contacting devices, the bare Ti surface activates the intrinsic pathway of coagulation and promotes unnecessary protein adsorption due to the negative surface charge [4]. Therefore, the achievement of an implant surface which enhances the biocompatibility while inhibiting protein adsorption and cell adhesion for preventing undesirable responses towards implants in living systems can potentially have biomedical application.

Modifications of biomaterial surfaces have a long history in implantology and form a major area of research. Among the considerable number of biomaterials that have been developed thus far, the phospholipid polymers prepared from 2-methacryloyloxyethyl phosphorylcholine (MPC) and other vinyl compounds have shown the greatest promise; they mimic the natural cell membrane surface and are, therefore, inherently resistant to biofouling by proteins. Moreover, it is known as they perform better than most other types of polymeric materials with respect to their resistance to protein adsorption, cell adhesion, and whole blood coagulation. For these reasons, MPC polymers are currently being widely used in the biomedical field for surface modification [5–16].

Since its introduction by Decher in 1992 [17,18], the process of building up organic multilayer films through layer-by-layer self-assembly (LbL) has been attracted a great deal of attention and allows the formation of interpolymer complexes by the deposi-

* Corresponding author at: Department of Materials Engineering, The University of Tokyo, 7-3-1, Hongo, Bunkyo-ku, Tokyo 113-8656, Japan. Fax: +81 3 5841 8647.
E-mail address: ishihara@mpc.t.u-tokyo.ac.jp (K. Ishihara).

0927-7765/$ – see front matter © 2008 Elsevier B.V. All rights reserved.
doi:10.1016/j.colsurfb.2008.08.025

tion of oppositely charged polyelectrolytes. The LbL method is renowned for being a convenient, versatile, and efficient technique to generate biologically active surfaces. In addition, compared with conventional polymer coating, it affords more stable coating and various applications because of chemical bonding between layer to layer, such as controlled drug release [19], cell–surface interaction [20] and surface modification [21]. Furthermore, various driving forces have been introduced for forming multilayers by the LbL method, such as electrostatic interaction [22–24], hydrogen bonding [25–28], and covalent bonding [29].

This study employed covalent bonding-driven self-assembly to produce polymer hydrogel multilayers on Ti surfaces. We adopted a phospholipid polymer (PMBV) containing 2-methacryloyloxyethyl phosphorylcholine, *n*-butyl methacrylate (BMA), and 4-vinylphenylboronic acid unit (VPBA). The hydrophobic BMA unit can regulate the solubility of MPC polymer and also form the hydrophobic domain in aqueous condition, which dissolve hydrophobic bioactive agents, such as paclitaxel [11]. Phenylboronic acid in a tetrahedral anionic structure is known to rapidly form a cyclic boronic complex with cis-diols [30], for example, carbohydrates such as glucose, catechol derivatives such as dopamine, and some polymers such as poly(vinyl alcohol) (PVA) [31,32]. The interpolymer complexation of a polymer comprising boronic acid with PVA has been reported to form a hydrogel due to the covalent linkage in both constituent polymers and this hydrogel is reversibly dissociated by the addition of glucose [33–35].

We expected that the LbL deposition method would enable the combination of PMBV and PVA to produce a polymer hydrogel multilayer bonded to Ti. Therefore, the objective of this study was to fabricate and characterize Ti surfaces modified with PMBV and PVA via the LbL method for improving biocompatibility of Ti implant. By constructing a multilayered hydrogel on the Ti surface, the surface may become much more biocompatible, and moreover, the multilayered hydrogel layer can have a functional stage for the sustained release of biologically active molecules.

2. Experimental

2.1. Materials

MPC was obtained from NOF (Tokyo, Japan); it was synthesized using a method proposed by Ishihara et al. [5]. *n*-Butyl methacrylate was purchased from Nacalai Tesque Co. Ltd. (Tokyo, Japan). VPBA and PVA (degree of polymerization: 1500) were purchased from Wako Pure Chemical Industries, Ltd. (Osaka, Japan). Octadecyltriethoxysilane (ODS) were purchased from ShinEtsu Chemical Co. Ltd. (Tokyo, Japan). Photoreactive PVA (AWP, azide-unit pendented water-soluble PVA) was purchased from Toyo Gosei Co. Ltd., Japan. Titanium alloy (Ti) substrates were obtained from DENISPY-Sankin K.K. (Tokyo, Japan). The other reagents and solvents were of the extra-pure grade and were used without further purification.

2.2. Synthesis of PMBV

PMBV was synthesized by the conventional radical polymerization of the corresponding monomers: the desired amounts of MPC, BMA, and VPBA were dissolved in ethanol taken in an ampoule. The total concentration of monomer was adjusted to 1.0 mol/L. An initiator, α,α′-azobisbutyronitrile (AIBN), was added to the ampoule at a concentration of 1.0 mmol/L. Next, argon gas was bubbled into the solution for 10 min to eliminate oxygen and the ampoule was then sealed. Polymerization was carried out at 60 °C for 2.5 h. After cooling, the contents were poured into a large amount of diethylether and chloroform (8:2 by volume) to remove any unreacted monomers and to yield PMBV. The precipitant was collected and dried *in vacuo*. The structure of the copolymer was confirmed with ^{1}H-NMR (α-300, JEOL, Tokyo, Japan) and a Fourier-transform infrared spectrometer (FT-IR; FT/IR-615, JASCO, Tokyo, Japan). The molecular weight was determined by gel permeation chromatography (GPC, JASCO, Tokyo, Japan). The chemical structure of PMBV is shown in Fig. 2.

2.3. Fabrication of multiplayer

2.3.1. Preparation and cleaning of Ti

Two types of Ti substrates were used. The Ti substrates were prepared from a Ti plate (thickness: 0.5 mm) by cutting it into 10 mm × 10 mm square pieces.

These were rinsed in acetone and ethanol using sonification for 15 min each. After drying in air, the samples were oxidized as follows: They were immersed in a 3:1 (v/v) mixture of concentrated H_2SO_4 and 30% H_2O_2 for 1 h at 25 °C. The samples were then rinsed three times with distilled water and dried in an oven at 60 °C. To evaluate the thickness of the multilayered hydrogel, quartz substrates (10 mm × 15 mm × 0.8 mm; Matsunami, Tokyo, Japan) were coated with a 100-nm-thick Ti layer by RF magnetron sputtering (Ulvac Kiko, Inc., Tokyo, Japan, duration: 4 min, pressure: ~2×10^{-3} Pa). The quartz substrates were cleaned using an oxygen plasma apparatus (PR500 plasma reactor, Yamato Science, Tokyo, Japan) for 20 min. Finally the Ti-sputtered substrates were oxidized using the oxygen plasma apparatus for 10 s, and silanization was carried out immediately afterward.

2.3.2. Silanization on Ti substrate

A monolayer of ODS was prepared by the following procedure: First, 10 mM ODS was dissolved in anhydrous toluene. The Ti substrates were then immersed in the ODS solution and reacted for 24 h at 80 °C. And finally, the Ti substrates were rinsed in toluene three times and dried *in vacuo* at room temperature.

2.3.3. Fabrication of multilayer on Ti substrate

The ODS-treated Ti substrates were coated with an aqueous solution of AWP (1 wt%) by dip coating. The AWP-coated Ti substrates were air-dried under a fume hood at room temperature. After applying the AWP coating, the Ti substrates were irradiated with UV light (135 mW/cm^2) using a UV Spot Cure (SP-7, Ushio Inc., Yokohama, Japan) for 40 s.

PMBV solutions with concentrations of 50 and 25 mg/mL and PVA solutions with concentrations of 15 and 30 mg/mL were prepared with distilled water. The combinations of PMBV and PVA solutions examined are as follows: PMBV 50 mg/mL and PVA 15 mg/mL (PMBV50/PVA15), PMBV 25 mg/mL and PVA 30 mg/mL (PMBV25/PVA30), and PMBV 25 mg/mL and PVA 15 mg/mL (PMBV25/PVA15). The multilayer construction was accomplished by alternately dipping the Ti substrates with bonded AWP in the PMBV and PVA solutions for 10 min each and subsequently rinsing them with distilled water for 1 min. Six layers (3-bilayers) terminated with a layer of PMBV were obtained by the LbL method.

2.4. Characterization of multilayers

The thickness of the polymer multilayer was characterized by field emission scanning electron microscopy (FE-SEM, S-4200, Hitachi, Japan). Multilayers were built up as described above on the surface of the Ti-sputtered quartz substrates. And the cross-section of the quartz substrate was analyzed after the formation of each layer. Gravimetric measurements were performed after each successive layer was constructed. The swelling ratios of the multilayered hydrogel on the Ti surface were obtained at room

temperature. Multilayered hydrogels in triplicate were incubated in phosphate-buffered saline (pH 7.4) and their dry weights were measured beforehand. Then, the swelling ratios were calculated by the following equation:

$$\text{Swelling ratio}(\%) = \left[\frac{(W_s - W_d)}{W_d}\right] \times 100$$

where W_s and W_d are the weights of the swollen and dry hydrogel, respectively.

The static water contact angle on the prepared surfaces was measured using the sessile drop method at the ambient temperature using a contact angle goniometer (G-1, Erma, Tokyo, Japan). Images of water spreading on the sample surfaces were recorded by a camera and then analyzed using the software supplied by the manufacturer. Five measurements were made for each sample. For captive bubble method, the glass cell was filled with ultrapure water and 1 cm^2 samples of test solids were placed in it. A special L shaped syringe needle containing air releases bubbles beneath the sample. A computer screen provided an image of the captive bubble and then analyzed using the software supplied by the manufacturer. In addition, infrared spectral analysis was performed by attenuated Fourier-transform infrared spectroscopy (ATR-FTIR, IMV-4000, FT/IR-6300, JASCO, Tokyo, Japan). The spectra were examined visually, with special interest given to the spectral range of 4000–850 cm^{-1}.

For chemical composition analysis, specimens were characterized using X-ray photoelectron spectroscopy (XPS; AXIS-His165 Kratos/Shimadzu, Kyoto, Japan) with a focused monochromatic Mg Kα X-ray source (1253.6 eV) for excitation. The electron take-off angle was 60° in the dry state and the analyzer was operated in the constant energy mode for all measurements.

2.5. Cell culture and cell morphology

For cell adhesion, L929 cells were cultured in a culture medium (D-MEM (Gibco), supplemented with 10% (v/v) fetal calf serum (FBS)) at 37 °C in an atmosphere of 5% CO_2 at 95% humidity. The cells were seeded at a density of 4×10^4 cells/mL on the experimental substrates and were cultured for 1 day. Subsequently, cell fixation was carried out for 90 min in 2.5% glutaraldehyde solution at 4 °C. Then, the samples were washed twice with PBS and dehydrated using a graded series of ethanol solutions (70%, 90%, and 100%) for 15 min each and were subsequently dried with 1,1,1,3,3,3-hexamethyldisilane. The morphology of the adherent cells was observed using a scanning electron microscope (SEM, SM-200, Topcon, Tokyo, Japan) after depositing gold.

3. Results

3.1. Characterization of PMBV

The copolymerization of MPC, BMA, and VPBA proceeded well and a polymer containing these monomer units was obtained; the obtained PMBV was water-soluble. The spectral data from ^{1}H-NMR and FT-IR revealed the chemical structure of the obtained PMBV.

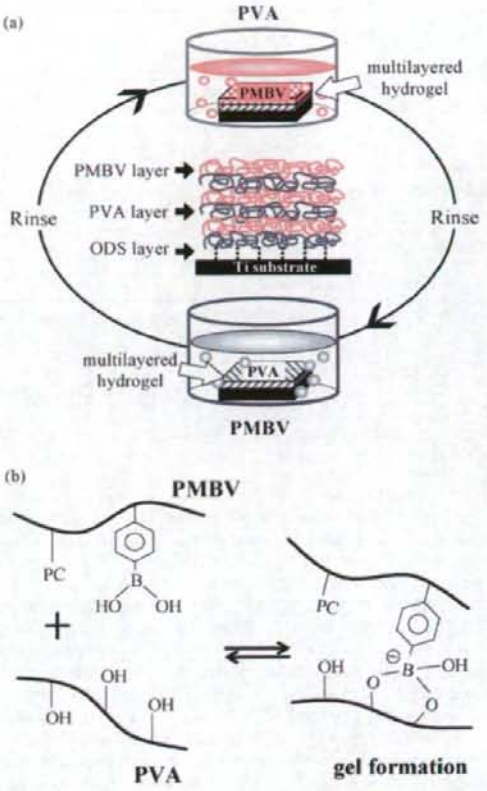

Fig. 1. (a) Schematic representation of construction procedure for the multilayered hydrogels on the Ti substrates. (b) Reaction between the phenylboronic acid moiety in PMBV in an aqueous solution and a polyol moiety in the presence of PVA.

Fig. 1 shows a schematic illustration of the process for fabricating the multilayered hydrogels on the Ti substrates via the LbL method (a) and the mechanism of PMBV/PVA hydrogel formation (b). The chemical structure and synthetic results of the obtained PMBV are summarized in Fig. 2 and Table 1.

3.2. Multilayered hydrogel formation from PMBV/PVA system

The preparation of the PMBV/PVA hydrogel layers on the Ti substrates via the LbL method was followed by a change in the weight

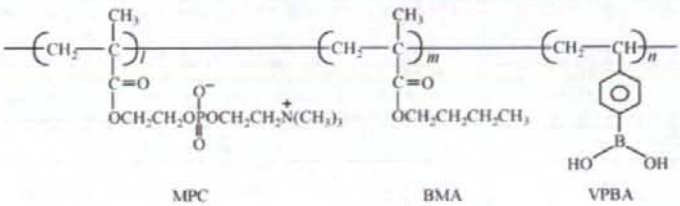

Fig. 2. Chemical structure of PMBV.

Table 1
Synthetic result of PMBV.

Abb	Monomer unit composition (mol%)[a]		Yield(%)	Molecular weight Mw($\times 10^4$)[b]
	In feed MPC/BMA/VPBA	In polymer MPC/BMA/VPBA		
PMBV	60/30/10	57/25/18	70	6.5

$[Monomer]_{total}$ = 1.0 mol/L in EtOH; [AIBN]=1 mmol/L; copolymerization time: 2.5 h, polymerization temperature 60 °C.
[a] Determined by ^{1}H-NMR.
[b] Determined by GPC.

Table 2
Characterization of polymer multilayer.

Polymer concentration (mg/mL) [PMBV]/[PVA]	Cumulative weight increase (mg) ± SD			Swelling ratio ± SD (%)
	Number of layer			
	2	4	6	
50/15	0.19 ± 0.01	0.96 ± 0.10	1.98 ± 0.23	440 ± 70
25/15	0.20 ± 0.14	0.31 ± 0.23	0.74 ± 0.42	340 ± 50

of the substrates; the results are shown in Table 2. Weight measurements showed an increase in the multilayered hydrogel on the Ti surface as a function of even numbers of coating layers. The cumulative weights of PMBV50/PVA15 and PMBV25/PVA15 after the formation of the 3-bilayer were measured as 1.98 ± 0.23 and 0.74 ± 0.42 mg, respectively. Moreover, the swelling ratios of the 3-bilayer hydrogels from the dried state in an aqueous medium were estimated by the weight change after allowing equilibration for 1 day; the results are shown in Table 2. PMBV50/PVA15 exhibited a higher swelling ratio than PMBV25/PVA15; the former exhibited a swelling ratio of 440 ± 70% and the latter, 340 ± 50%. The ATR-FTIR spectrum of each outer layer formed during the fabrication process is shown in Fig. 3. As the specific surfaces changed gradually from Ti to PMBV, each spectrum expressed the particular peaks associated with the functional groups of that surface. After the bare Ti surface (Fig. 3(a)) treated the silanization, the ODS-treated Ti surface (Fig. 3(b)) exhibited the band corresponding to ≡Ti–O–Si≡ in the region of 970–1000 cm^{-1}. And

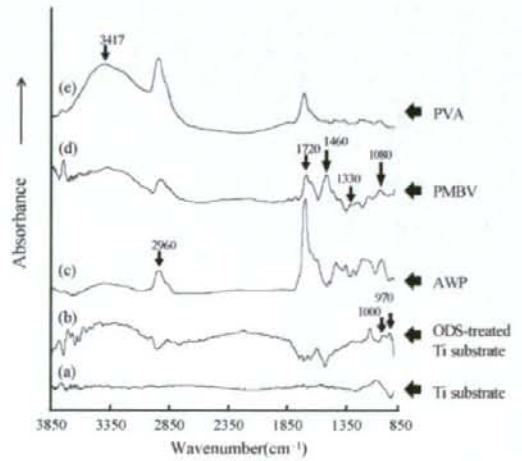

Fig. 3. ATR-FTIR spectra of (a) Ti substrate, (b) ODS-treated Ti substrate, (c) AWP, (d) PMBV, and (e) PVA. In this case, the multilayered hydrogel of PMBV25/PVA30 was used.

after bonding the AWP layer (Fig. 3(c)) to the ODS-treated Ti surface, the spectrum exhibited characteristic vibration at 1720 cm^{-1} for the carbonyl group, and at 1650 and 1463 cm^{-1} for the C=C of aromatic ring. However, no azide peak was observed around 2200 cm^{-1}. After complexation with PMBV (Fig. 3(d)), the phosphate group in the MPC unit could be seen at 1080 and 970 cm^{-1}, and peaks at 1720 and 1460 cm^{-1} corresponding to C=O carbonyl stretching and $-CH_2-$ bending were also observed, respectively. The appearance of peaks at 1330 and 1350 cm^{-1} is attributed to the B–O stretching modes in phenylboronic acid. In Fig. 3(e), the peak around 3417 cm^{-1} is associated with the –OH bands in PVA. The thickness of the PMBV/PVA hydrogel increased as a function of the number n of deposited layers (Fig. 4). The final thicknesses of PMBV50/PVA15, PMBV25/PVA30, and PMBV25/PVA15 were determined as 8, 7, and 6 μm by SEM measurements of the cross-sections of the hydrogel layers on the Ti-sputtered quartz, respectively.

3.3. Surface property of the multilayered hydrogel

The contact angle depends on the character of surface wettability, and measurements were performed to confirm the alternate deposition of PMBV and PVA. Polymer hydrogel layers made by layer-by-layer methods on Ti surfaces are expected to alternately change surface wettability. Fig. 5 shows the results of the static water contact angle by sessile drop method and by the captive bubble method for three polymer combinations. In case of the sessile drop method (Fig. 5(a)), the static water contact angle for PVA 15 and 30 mg/mL is approximately 60°, and that for PMBV 25 and 50 mg/mL is 80°. The subsequent adsorption of PMBV made the surface slightly hydrophobic compared to that with the PVA surface in dry condition. However, in the case of captive bubble method (Fig. 5(b)), while PVA layers are approximately 40°, most of PMBV layers are 20° and all of the 6th layers are 0° regardless of PMBV concentrations. This means the outmost layers of multilayered hydrogel are totally covered with PMBV. The alternation of the static contact angle and captive bubble contact angle strongly indicates that the hydrogel layers were constructed regularly. XPS is useful tool for obtaining qualitative and quantitative information of the different elements at a substrate surface. XPS was used to monitor each deposition step as it can provide information on the surface phosphorus/carbon ratio (P/C ratio) on the Ti samples coated with different deposition layers; the results are

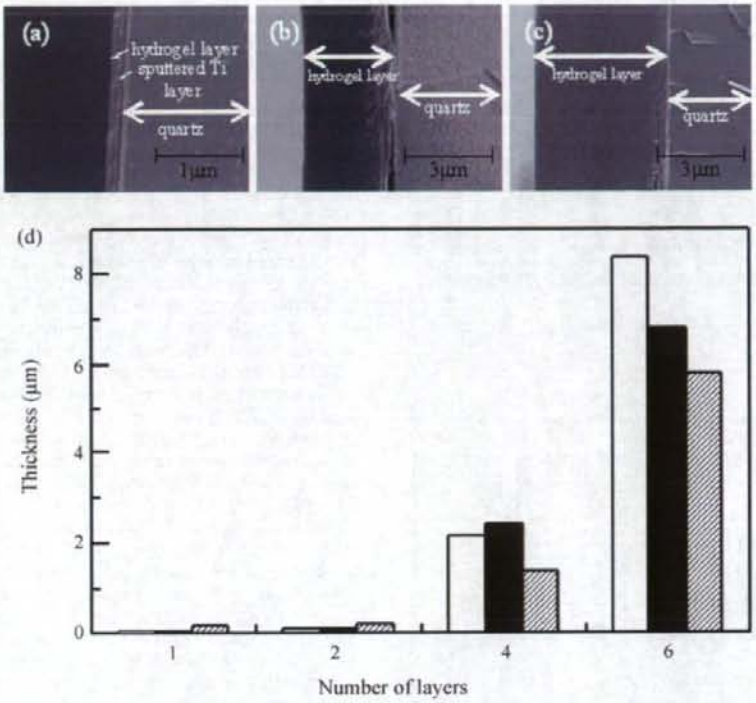

Fig. 4. Cross-sectional SEM images of multilayered hydrogel with (a) second layer (b) fourth layer, and (c) sixth layer of PMBV25/PVA30. (d) Hydrogel layer thickness of PMBV/PVA measured by SEM as a function of layer number. In this case, samples with an even number of layers have PMBV, whereas samples with an odd number of layers have PVA: (□) PMBV50/PVA15, (■) PMBV25/PVA30, and (▨) PMBV25/PVA15. Multilayered hydrogels were constructed on Ti-sputtered quartz substrates. The results are the means of the results of three independent experiments.

presented in Fig. 6. As the deposition cycle was repeated, P/C ratio could discriminate the presence or absence of a PMBV layer; that is, PMBV-terminated layers (the even number) exhibited 4 times larger P/C values.

3.4. Cell adhesion on the multilayered hydrogel

The morphological aspects of L929 cells grown on the differently loaded multilayered hydrogel coatings were evaluated using an SEM (Fig. 7). On a plain Ti substrate (Fig. 7(a,b)) and on one modified with AWP (Fig. 7(c,d)), the adhesion and proliferation of L929 cells was observed during a 1-day culture, as usual. However, apparent differences in cell morphology were found on PMBV (Fig. 7(e,f)) and PVA (Fig. 7(g,h)) as compared to that on the Ti substrate and AWP-modified substrate. That is, the number of L929 cells that adhered to the PMBV and PVA surfaces was significantly lesser than those on the Ti substrate and photoreactive PVA. In addition, the L929 cells did not preserve their normal spindlelike shape, but exhibited circular, round shapes.

4. Discussion

This study focused on the fabrication and characterization of multilayered hydrogels using water-soluble MPC polymers bearing a phenylboronic acid moiety and PVA via the LbL deposition method. Phenylboronic acid is one of the most familiar reactive groups used to synthesize stable covalent complexes with polyol compounds, including PVA. Because of the strong binding, it can be used as a recognition moiety in sugar fractionation. However, besides sugar recognition, the usage of polyols such as PVA has permitted the present system to form hydrogels without any chemical crosslinking treatment. Moreover, the use of PVA in hydrogels has attracted considerable attention because of its inherent low toxicity and high degree of swelling in water [33]. The LbL method is a desirable and versatile tool for assembling PMBV and PVA into a multilayered hydrogel. In this study, we have chosen the concentration of polymer capable of forming hydrogel upon mixing aqueous solutions in physiological condition, whose conditions depend on the concentrations of PMBV and PVA. The gelation did not affect the ionic strength [34]. After constructing multilayered hydrogel, we observed the chemical bonding between layer to layer through unique peaks of FT-IR. However, it was not clear to confirm the bonding between phenylboronic acid and polyol because the change of peak corresponding to –B–O stretching appeared from 1330 to 1350 cm^{-1}.

Based on the increases in both the weight and thickness of the substrates, we confirmed that the LbL method was feasible with the PMBV/PVA system. The build-up of multilayered films arises from covalent bonding between alternately deposited PMBV and PVA. In case of thickness, the concentration of AWP coated on Ti substrate was lower than that of PMBV and PVA constructing multilayer by LbL method, that is, the number of binding sites are different. This is why the difference of thickness between 1st layer and 2nd layer

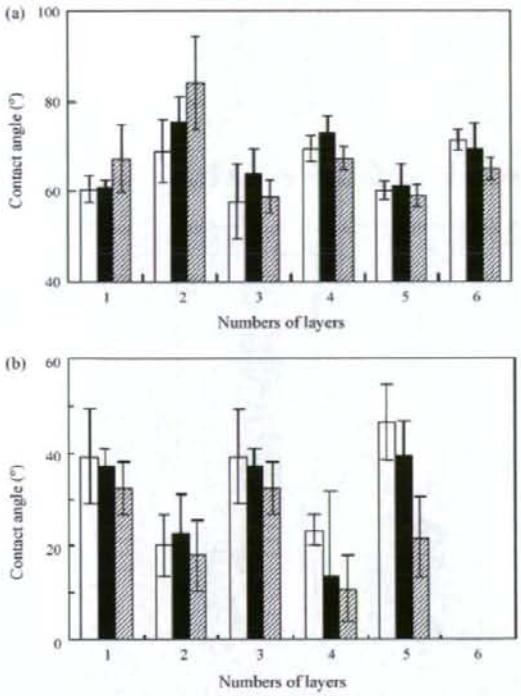

Fig. 5. The static water contact angles (a) by sessile drop method and (b) by captive bubble method on the PMBV/PVA multilayered hydrogel surface as a function of the layer number. In these cases, samples with an even number of layers have PMBV, whereas samples with an odd number of layers have PVA: (□) PMBV50/PVA15, (■) PMBV25/PVA30, and (▨) PMBV25/PVA15. The results are expressed as the mean ± SD for three independent experiments.

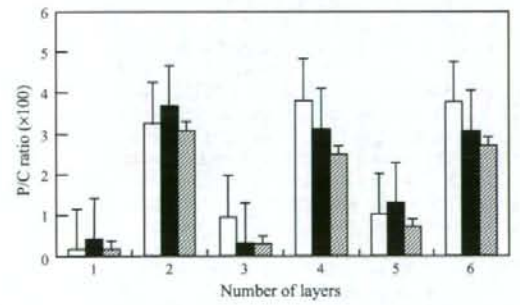

Fig. 6. P/C ratio of multilayered PMBV/PVA hydrogel layer. The even numbers correspond to PMBV as the outmost layer and the odd numbers correspond to PVA as the outmost layer: (□) PMBV50/PVA15, (■) PMBV25/PVA30, and (▨) PMBV25/PVA15. The results are expressed as the mean ± SD for three independent experiments.

cannot observe. From 2nd layer to 6th layer, the thicknesses have increased linearly and have been influenced in the concentration of polymers. The number of cycles and the concentrations of polymer solution modulate the thickness [24,35]. The change in both weight and thickness of the hydrogel layer depend on the polymer concentrations. PMBV/PVA multilayered hydrogel appeared high swelling ratio without regard for polymer concentration. It means both of PVA and PMBV containing hydrophilic PC-group are familiar to water molecules. It is thought that the contact angle data also support hydrophilic property of these polymers. Both of the contact angle measurement revealed that the outmost layer was exchanged alternatively. In particular, as the captive bubble method indicates the wettability of surface in wet condition, we could obtain interesting information by comparing the results of the sessile drop method. When the outermost layer was PMBV, the contact angle in dry condition increased over that with PVA. This means the surface of PMBV layer is covered with hydrophobic group, that is, phenylboronic acid and butyl group of BMA. However, the contact angle of PMBV in wet condition is dramatically opposed to that in dry condition. It is due to the rapid adsorption of the water molecules around the hydrophilic PC-groups in the PMBV [36]. In all of case, the contact angle of 6th layer is zero (Fig. 5(b)). It is thought that the outmost surfaces are covered with PMBV. On the other hand, PVA layers keep similar surfaces covered with hydroxyl groups regardless of whether it is in dry condition or it is in wet condition. From both of contact angle data, although it is known that PC-containing polymer, PMBV, and PVA are hydrophilic, we could observe the change of surface property in dry and wet condition. According to the change of layer surface from PVA to PMBV, the P/C ratio in XPS increased because of the influence of PMBV, which contains a phosphorylcholine group. The measurements of the static contact angle and the XPS results are susceptible to the surface property. In addition, the ATR-FTIR data showed that the Ti substrates were connected to the organic polymer material by silanization and photoreaction with AWP. Although the infrared spectral criterions of the azide structure have a characteristic around 2200–2300 cm^{-1}, it was thought that no trace was observed because ODS and AWP were bonded together by UV irradiation.

The cellular behavior is an important factor for interpreting the biocompatibility of biomaterial. The cell morphology images revealed that Ti and AWP surfaces permitted the adhesion, spreading, and migration of L929 cells to degrees that PVA and PMBV surfaces did not. The adhesion of cells to surfaces is dependant on the adsorption of highly adhesive proteins such as fibronetin and vitronectin, which link cells to the biomaterial surface. Cell–substrate interaction is mainly based on the recognition of Arg-Gly-Asp (RGD) sequences by receptors located on the cell surface. As AWP allows easy immobilization of specific proteins, it has been studied for application to microarray chips and cell adhesion assays [37]. It is generally accepted that hydrophilic polymers such as poly(ethylene oxide)-based polymers and phosphorylcholine-functioned polymers do not allow protein adsorption at their surface. Thus, they can reduce the adhesion of cells, including fibroblasts, platelets, and macrophages [9,10,38]. A wide variety of polymers containing charges, including anionic DNA and cationic chitosan, have been used for the construction of multilayerd coatings with the aim to modulate cell behavior. In particular, various studies with cells, including fibroblast and osteoblast, have shown that polyelectrolyte multilayered coatings are useful tool to regulate biomaterial surface through in vitro experiment of cell proliferation and viability [21,39]. In this study, the MPC polymer-hybridized Ti substrates and multilayered hydrogels offer the potential for preparing blood-contacting materials via the incorporation of the outmost layer, PMBV, which inhibits the adsorption of proteins and the adhesion of cells. Moreover, we note that bioactive reagents may be incorporated in the multilayered hydrogel to allow for sustained release using hydrophobic domain of BMA unit. Hence, the release behavior of a bioactive reagent from a Ti substrate with an immobilized hydrogel is currently under investigation in the laboratory and the results will be reported in the near future.

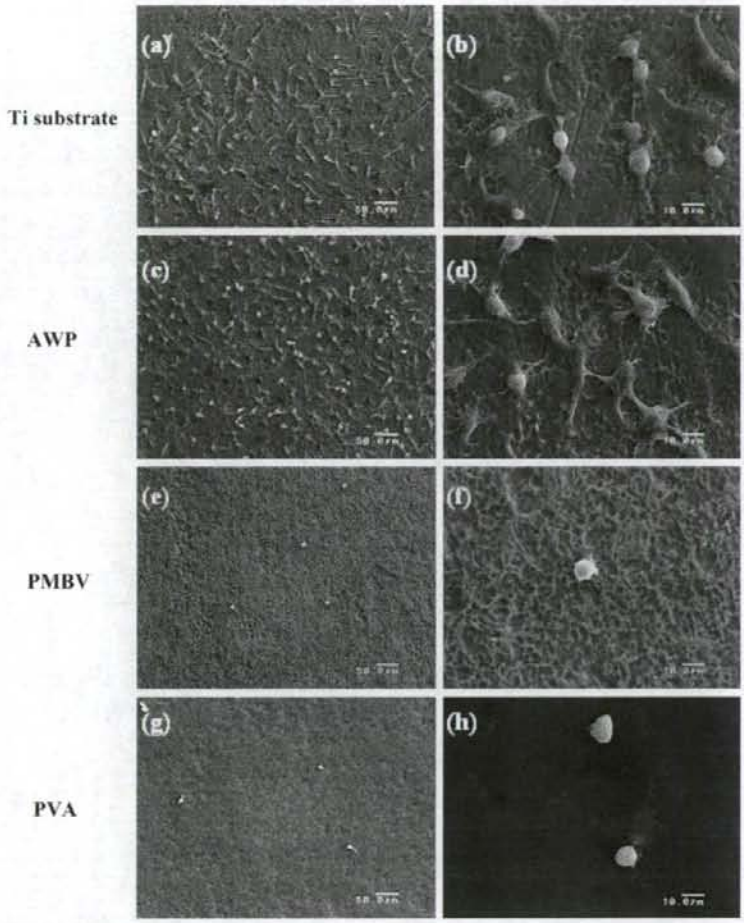

Fig. 7. SEM images of L929 cell morphology adhered on a Ti substrate (a, b) and on Ti substrates modified with AWP (c, d), PMBV (e, f), and PVA (g, h) after a 1-day culture. The PMBV and PVA concentration were 25 and 30 mg/mL, respectively.

5. Conclusions

This study demonstrates the feasibility of the LbL method in constructing multilayered hydrogels composed of the PMBV/PVA system on Ti substrates for improving biocompatibility of implant surface. The basic mechanism for the construction of the multilayered hydrogels was the selective reactions between the boronic acid moiety in PMBV and the hydroxyl groups in PVA. To initiate the LbL process, a silane coupling reaction was used to introduce an alkyl group on the Ti substrates, and AWP could bind covalently to the substrate surface by photoirradiation. Subsequently, the PMBV/PVA hydrogel system was fabricated. The process was followed by contact angle measurements and XPS analyses; these results indicated that the surface properties changed alternatively, reflecting the nature of the polymer on the outer surface. The thickness of the hydrogel increased with the number of layers. These data suggested that PMBV/PVA successfully covered the Ti substrate surface. Furthermore, PMBV, the outmost layer, was found to inhibit cell attachment. Moreover, the hydrogel layer can effectively entrap bioactive reagents and control their diffusivity. Research on this is currently underway in our laboratory and the results will be reported in the near future.

We concluded that the Ti substrates with multilayered polymer hydrogels will be useful in applications such as implantable devices and local drug delivery systems.

Acknowledgment

This study was partially supported by the Mitsubishi Foundation (Research grants in the natural sciences) in 2007.

References

[1] B. Kasemo, Surf. Sci. 500 (2002) 656.
[2] S. Tosatti, S.M. De Paul, A. Askendal, S. VandeVondele, J.A. Hubbell, P. Tengvall, M. Textor, Biomaterials 24 (2003) 4949.
[3] P.H. Chuna, K.G. Neoh, E.T. Kang, W. Wilson, Biomaterials 29 (2008) 1412.
[4] X. Liu, P.K. Chub, C. Dinga, Mater. Sci. Eng., R 47 (2004) 49.
[5] K. Ishihara, T. Ueda, N. Nakabayashi, Polym. J. 22 (1990) 355.
[6] T. Ueda, H. Oshida, K. Kurita, K. Ishihara, N. Nakabayashi, Polym. J. 24 (1992) 1259.

[7] K. Ishihara, N.P. Ziats, B.P. Tierney, N. Nakabayashi, J.M. Anderson, J. Biomed. Mater. Res. 25 (1991) 1397.
[8] K. Ishihara, H. Oshida, Y. Endo, T. Ueda, A. Watanabe, N. Nakabayashi, J. Biomed. Mater. Res. 26 (1992) 1543.
[9] K. Ishihara, H. Nomura, T. Mihara, K. Kurita, Y. Iwasaki, N. Nakabayashi, J. Biomed. Mater. Res. 39 (1998) 323.
[10] Y. Iwasaki, A. Mikami, N. Yui, K. Ishihara, N. Nakabayashi, J. Biomed. Mater. Res. 36 (1997) 508.
[11] T. Konno, J. Watanabe, K. Ishihara, J. Biomed. Mater. Res. 65A (2003) 209.
[12] T. Moro, Y. Takatori, K. Ishihara, T. Konno, Y. Takigawa, T. Matushita, U.I. Chung, K. Nakamura, H. Kawaguchi, Nat. Mater. 3 (2004) 829.
[13] J. Sibarani, M. Takai, K. Ishihara, Colloid Surf. B 54 (2007) 88.
[14] Y. Xu, M. Takai, T. Konno, K. Ishihara, Lab Chip 7 (2007) 199.
[15] K. Nishizawa, T. Konno, M. Takai, K. Ishihara, Biomacromolecules 9 (2008) 403.
[16] J.H. Seo, R. Matsuno, T. Konno, M. Takai, K. Ishihara, Biomaterials 29 (2008) 1367.
[17] G. Decher, J.D. Hong, J. Shimit, Thin Solid Films 210 (1992) 831.
[18] G. Decher, Science 277 (1997) 1232.
[19] M.C. Berg, L. Zhai, R.E. Cohen, M.F. Rubner, Biomacromolecules 7 (2006) 357.
[20] T. Serizawa, M. Yamaguchi, T. Matsuyama, M. Akashi, Biomacromolecules 1 (2000) 306.
[21] K. Cai, A. Rechtenbach, J. Hao, J. Bossert, K.D. Jandt, Biomaterials 26 (2005) 5960.
[22] F. Caruso, K. Niikura, N.D. Furlong, Y. Okahata, Langmuir 16 (2000) 1249.
[23] S.S. Shiratori, M.F. Rubner, Macromolecules 33 (2000) 4213.
[24] K. Ren, J. Ji, J. Shen, Biomaterials 27 (2006) 1152.
[25] W.B. Stockton, M.F. Rubner, Macromolecules 30 (1997) 2717.
[26] J.F. Quinn, F. Caruso, Adv. Funct. Mater. 16 (2006) 1179.
[27] S.A. Sukhishvili, S. Granick, Macromolecules 35 (2002) 301.
[28] E. Brynda, M. Houska, J. Colloid Interface Sci. 183 (1996) 18.
[29] J. Yan, G. Springsteen, S. Deeter, B. Wang, Tetrahedron 60 (2004) 11205.
[30] Y. Ma, L. Qian, H. Huang, X. Yang, J. Colloid Interface Sci. 295 (2006) 583.
[31] A. Matsumoto, S. Ikeda, A. Harada, K. Kataoka, Biomacromolecules 4 (2003) 1410.
[32] S. Kitano, I. Hisamitsu, Y. Koyama, K. Kataoka, T. Okano, Y. Sakurai, Polym. Adv. Technol. 2 (1991) 261.
[33] P.R. Hari, K. Sreenivasan, J. Appl. Polym. Sci. 82 (2001) 143.
[34] T. Konno, K. Ishihara, Biomaterials 28 (2007) 1770.
[35] G. Ladam, P. Schaad, J.C. Voegel, P. Schaaf, G. Decher, F. Cuisinier, Langmuir 16 (2000) 1249.
[36] T. Goda, T. Konno, M. Takai, K. Ishihara, Colloids Surf. B: Biointerfaces 54 (2007) 67.
[37] Y. Ito, M. Nogawa, M. Takeda, T. Shinuya, Biomaterials 26 (2005) 211.
[38] K. Smetana Jr., Biomaterials 14 (1993) 1046.
[39] J.J.J.P. van den Beucken, X.F. Walboomers, M.R.J.N. Vos, A.J.M. Sommerdijk, R.J.M. Nolte, J.A. Jansen, J. Biomed. Mater. Res. 77A (2006) 202.

J Mater Sci: Mater Med (2008) 19:1009–1016
DOI 10.1007/s10856-007-3076-8

Mechanical, setting, and biological properties of bone cements containing micron-sized titania particles

Koji Goto · Masami Hashimoto · Hiroaki Takadama · Jiro Tamura · Shunsuke Fujibayashi · Keiichi Kawanabe · Tadashi Kokubo · Takashi Nakamura

Received: 18 January 2007 / Accepted: 3 April 2007 / Published online: 1 August 2007

Abstract In this study, polymethylmethacrylate-based composite cements containing 40–55.6 wt% micron-sized titania (titanium oxide) particles were developed, and their mechanical, setting, and biological properties evaluated. Three types of composite cement containing 40, 50, and 55.6 wt% silanized titania were designated ST2-40c, ST2-50c, and ST2-56c, respectively. In animal experiments, ST2-50c and ST2-56c were implanted into rat tibiae and solidified in situ. An affinity index was used to evaluate osteoconductivity. Compressive and bending strength of ST2-56c was 147.7 ± 3.2 and 69.3 ± 7.4; those of the other cements exceeded 100 MPa and 50 MPa, respectively. The affinity indices of ST2-56c were 42.1 ± 12.9 at six weeks and 53.4 ± 16.6 at 12 weeks, and were significantly higher than for ST2-50c and a commercial PMMA bone cement within 12 weeks. Our data indicate that bone cement containing micron-sized titania particles can be applied to prosthesis fixation as well as vertebroplasty, and ST2-56c is a good candidate cement.

K. Goto (✉) · J. Tamura · S. Fujibayashi · K. Kawanabe · T. Nakamura
Department of Orthopaedic Surgery, Faculty of Medicine, Kyoto University, Kawahara-cho 54, Shogoin, Sakyo-ku, Kyoto 606-8507, Japan
e-mail: k.g.bau@kuhp.kyoto-u.ac.jp

M. Hashimoto · H. Takadama
Japan Fine Ceramics Center, Mutsuno 2-4-1, Atsuta-ku, Nagoya 456-8587, Japan

T. Kokubo
Research Institute for Science and Technology, Chubu University, 1200 Matsumoto-cho, Kasugai 487-8501, Japan

Introduction

Since the 1990s, many types of bioactive bone cement have been developed to overcome the disadvantages of polymethylmethacrylate (PMMA) bone cement [1], especially its lack of bone-bonding ability, which occasionally leads to aseptic loosening of prostheses used for arthroplasty [2, 3]. However, the acceptable long-term clinical results of PMMA bone cement [4, 5], and concerns about the long-term stability of bioactive fillers in the cements have so far prevented bioactive bone cements being used for the fixation of prostheses in arthroplasty. Recently, anatase and rutile, crystal phases of titania, have been shown to have excellent in vitro apatite-forming ability and in vivo bioactivity [6–9]. Titania is stable in the body and does not degrade, so that bone cements containing bioactive titania filler can be stable in the body environment. Then a composite bone cement containing nanosized anatase-type titania particles was developed, and it was reported that certain compositions of the cement had good osteoconductivity [10]. However, some of the nanosized titania particles tended to aggregate in the cement. As a result, the cements containing nanosized titania particles did not reach the minimum bending strength required by the ISO 5833 standard (50 MPa), which is applied to acrylic resin cements used for prosthesis fixation, and could be applied clinically for vertebroplasty, but not for prosthesis fixation. One possible resolution of this problem was to increase the titania particle size. In this study, composite cements that contained micron-sized titania particles were developed. Preliminary PMMA cement candidates with different amounts of titania particles were examined for their mechanical properties and apatite forming ability in vitro [11], and two promising composites were used in an implantation study.

The purpose of the study was to evaluate the mechanical and setting properties, and osteoconductivity of cements containing micron-sized titania.

Materials and methods

Preparation of powders

Titania powder

Plate-like titania powder (Ishihara Sangyo Kaisha, Osaka, Japan) with an average particle size of 1.55 μm was used as supplied. The particle size distribution of the titania powder, which was determined using a laser diffraction analyzer (LA-910; Horiba, Kyoto, Japan), is shown in Fig. 1a. Powder X-ray diffraction of the particles revealed that the titania particles were composed of anatase and rutile phases (Fig. 1b). The weight ratio of anatase:rutile in the 1.55 μm titania powder was about one, based on the peak intensities of each diffraction pattern. The titania powder was mixed into three types of TiO_2-dispersed cements with 40, 50, and 55.6 wt% TiO_2, designated ST2-40c, ST2-50c, and ST2-56c, respectively.

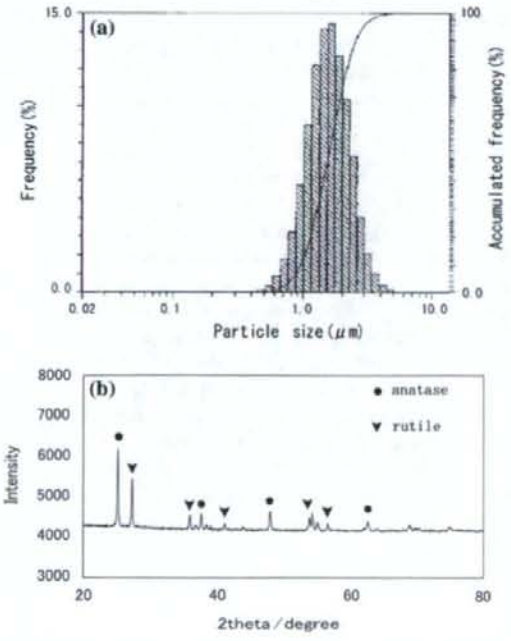

Fig. 1 (**a**) Titania powder particle size distribution. (**b**) Powder X-ray diffraction data for titania powder

Titania powders were treated with a silane-coupling agent as follows: 1.1 g of 3-methacryloxypropyltrimethoxysilane (Shin-Etsu Chemical Co., Tokyo), 1.6 g of ethanol and 0.2 g of deionized water were mixed on a magnetic stirrer for 10 min. The solution containing the silane-coupling agent was added to 110 g of the TiO_2 powder and mixed in a shaker mixer (TURBULA T2F, W. A. Bachofen AG Co., Basel, Switzerland) at 25 °C for 1 h. The rotation speed was 96 rpm. After mixing, the mixtures were dried and heated at 130 °C for 5 min.

Polymethylmethacrylate powder

Spherical PMMA powder, synthesized by suspension polymerization [12], with an average molecular weight of 270,000 Da and an average particle size of 5 μm (standard deviation: 2 μm) [13] was used.

Preparation of the liquid

Liquid methacrylate (MMA) monomer (Wako Pure Chemical Industries, Osaka, Japan) was used.

Cement preparation

Four types of cement, designated ST2-40c, ST2-50c, ST2-56c, and PMMAc, were prepared. PMMAc was a commercially available PMMA-based bone cement (Osteobond; Zimmer, Warsaw, IN, USA) and was used as a control material. The composition of each TiO_2-containing cement is shown in Table 1. As an initiator, benzoyl peroxide (Nacalai Tesque, Kyoto, Japan) was added to the powder at 4.0 wt% of the monomer, and as an accelerator, *N,N*-dimethyl-*p*-toluidine (Kanto Chemical Co. Inc., Tokyo, Japan) was dissolved in the liquid to 2.0 wt% of the monomer. Each cement was prepared by mixing the powder with the liquid for 1 min.

Mechanical testing

The compressive strength, bending strength, and bending modulus of ST2-40c, ST2-50c, and ST2-56c were mea-

Table 1 Composition of PMMA-based cements containing titania powders

Cement	Powders[a] (wt%)		Liquid[b] (wt%)
	Titania	PMMA	MMA
ST2-40c	40	20	40
ST2-50c	50	16.7	33.3
ST2-56c	55.6	14.6	29.6

[a] Benzoyl peroxide was added at 4 wt% of the MMA

[b] *N,N*-Dimethyl-*p*-toluidine was added at 2 wt% of the MMA

sured using five prehardened cement specimens for each mechanical test. For mechanical bending analysis, four-point bending testing was performed with rectangular specimens sized to 70 mm × 20 mm × 5 mm. For compressive mechanical analysis, prehardened cylindrical cement specimens, 6 mm in diameter and 12 mm in length, were prepared. The tests were carried out according to ISO 5833, with a Model 5582 testing machine (Instron Corporation, Canton, MA, USA); the test conditions were previously described in detail [10].

Some of the bending specimens were prepared for observation with a scanning electron microscope (SEM, S-4700; Hitachi, Tokyo, Japan), and the fracture surfaces were analyzed to determine the microstructure of the cements.

Setting of the cements

The cement pastes were mixed for 1 min and cast in a cylindrical mold made of polytetrafluoroethylene (inner diameter 60 mm, inner depth 20 mm). The temperature change during the setting reaction was measured using an infrared thermometer under ambient conditions of 23 °C and 54–65% humidity. By plotting the time and temperature, the setting time of each cement was determined according to ISO 5833.

Animal experiments

Eight-week-old male Wistar rats weighing 180–230 g were used for the implantation study. The animals were reared and the experiments carried out at the Institute of Laboratory Animals, Faculty of Medicine, Kyoto University, under the institutional guidelines for use of experimental animals set by Kyoto University.

The rats were operated on under general anesthesia induced by intraperitoneal injection of sodium 5-ethyl-5-(1-methylbutyl) barbiturate (Nembutal [pentobarbital]; Dainippon Pharmaceutical Company, Osaka, Japan) at 40 mg/kg of body weight. Cortical bone defects measuring 2 mm × 7 mm were created in the medial aspect of the proximal metaphyses of both tibiae, and the bone marrow was curetted. The intramedullary canals of both bone defects were irrigated with physiological saline, and paste-form cement was inserted manually and allowed to cure in situ for evaluation of osteoconductivity [10, 14, 15]. Twelve rats (24 legs) were used for the evaluation of osteoconductivity, with ST2-50c and ST2-56c each being used in 12 legs. Half the rats in each subgroup were killed at six and 12 weeks after the operation.

To confirm the high radiopacity of ST2-56c, another operation was performed using an additional rat. After a hole had been made in the intercondylar space of the distal femur, and the intramedullary canal of the total femur was curetted and irrigated with physiological saline, ST2-56c and PMMAc in liquid phase were inserted into each of the bilateral canals using a syringe fitted with an 18-gauge needle, and this was allowed to cure in situ. One day after the operation, the rat was killed and an X-ray radiograph of the femurs was taken.

Micrographic examination

Specimens were dehydrated through a graded series of ethanol (70, 80, 90, 99, and 100 vol%) and embedded in epoxy resin (Epofix, Struers Co., Copenhagen, Denmark). Thin sections (100 or 500 μm thick) were cut with a band saw (BS-3000; Exakt, Norderstedt, Germany) perpendicular to the axis of the tibias containing the cement. Four sections could be typically made from each leg. The third section (100 μm thick) from the most distal portion of each leg was ground to a thickness of 60–80 μm using a grinding–sliding machine (Microgrinding MG-4000; Exakt) for Giemsa surface staining. The second section (100 μm thick) from each leg was prepared for contact microradiography. The first and fourth sections (500 μm thick) from each leg were polished with diamond paper and coated with a thin layer of carbon for observation by SEM (S-4700, Hitachi, Tokyo, Japan). Some of those specimens were analyzed using an energy-dispersive X-ray microanalyzer (EMAX-7000; Horiba, Kyoto, Japan) attached to the SEM (SEM–EDX). To evaluate osteoconductivity, affinity indices (%) for each subgroup were calculated as previously described [10, 14, 15].

Statistical analysis

Values were expressed as means and standard deviations (SD). Values of mechanical properties for each cement and the affinity indices for each cement at each time interval were compared using one-way analysis of variance. Subsequently, possible differences were investigated using Fisher's PLSD post hoc statistical test using StatView (version 5.0) for Windows. A P value less than 0.01 was considered statistically significant.

Results

Mechanical properties

The results of the mechanical property measurement and their statistical analyses are shown in Table 2. The ultimate compressive strength, flexural strength, and flexural modulus increased as the titania content of the cement increased. SEM revealed that titania particles were

Table 2 Mechanical properties of ST2-40c, ST2-50c, ST2-56c, and PMMAc (means ± SD, $n = 5$)

	Compressive strength (MPa)	Bending strength (MPa)	Bending modulus (GPa)
ST2-40c	106.1 ± 5.5*	54.3 ± 6.6	3.10 ± 0.47
ST2-50c	127.9 ± 6.4*	57.8 ± 4.1	3.88 ± 0.46
ST2-56c	147.7 ± 3.2*	69.3 ± 7.4**	4.07 ± 0.83
PMMAc	87.9 ± 2.7*	59.4 ± 7.8	1.56 ± 0.28***

The values for PMMAc were derived from our previous study[10]

* All pairs were significantly different

** Significantly different to ST2-40c

*** Significantly different to all the other cements

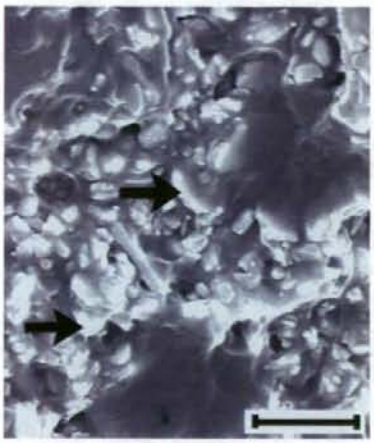

Fig. 2 Scanning electron micrograph of the fracture surface of ST2-56c. Arrows indicate titania particles. Bar = 3 μm

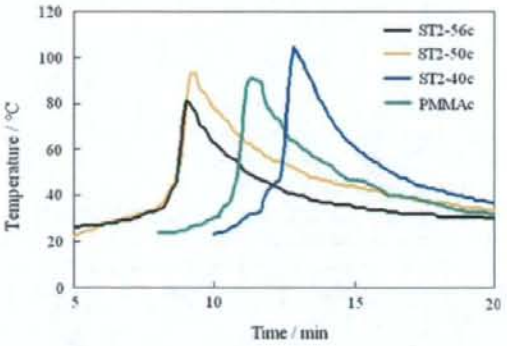

Fig. 3 Heat evolution curves for the setting reactions of ST2-50c, ST2-56c, PMMAc, and ST2-40c

uniformly dispersed and interacted well with the PMMA, and aggregates of titania particles could not be seen in the fracture surfaces of each cement (Fig. 2).

Setting time and peak temperature

The results of the temperature plotting of the cements are shown in Fig. 3. The setting times were 12 min 40 s for ST2-40c, 9 min 0 s for ST2-50c, 8 min 50 s for ST2-56c, and 11 min 0 s for PMMAc. The peak temperatures were 104 °C for ST2-40c, 93 °C for ST2-50c, 81 °C for ST2-56c, and 91 °C for PMMAc. The setting time of the cements containing titania particles reduced and the peak temperature decreased as the titania filler content increased.

Radiopacity

The ST2-56c in the femur was much more radiopaque than the PMMAc (Fig. 4). Both the ST2-56c and PMMAc were injected through an 18-gauge needle without problems, although ST2-56c was more easily injected.

Evaluation of the bone–cement interface

Giemsa surface staining indicated that there was typically no inflammatory reaction around ST2-50c and ST2-56c (Fig. 5a, b). The intervening soft tissue layer between cement and bone was more often seen around ST2-50c than ST2-56c at each time interval. For ST2-56c, no significant change in appearance could be seen with Giemsa surface staining between the 6- and 12-week specimens. On the other hand, for ST2-50c, there appeared to be less intervening soft tissue layer between the cement and bone in the 12-week specimens than in the 6-week specimens.

Low magnification SEM revealed that ST2-56c was in direct contact with bone over large areas within six weeks, whereas ST2-50c was in contact with bone in only small areas (Fig. 6a, b). In the 12-week specimens, both ST2-56c and ST2-50c were in direct contact with bone over large areas (Fig. 6c, d). Both ST2-50c and ST2-56c showed a marginal white line 30–60 μm wide at each time interval,

Fig. 4 X-ray radiograph of bilateral femurs of a rat one day after the operation

regardless of whether they were in contact with bone. These findings were also revealed by contact microradiography, in which each cement appeared to be in direct contact with bone over larger areas than in the SEM observation (Fig. 7a, b).

Backscattered SEM at high magnification revealed that both ST2-56c and ST2-50c were in direct contact with bone within six weeks, but a thin intervening soft tissue layer less than 10 μm thick was often observed between ST2-50c and the bone (Fig. 8a, b). It also showed that ST2-50c and ST2-56c were in contact with bone via a white line, which was demonstrated by SEM–EDX analyses to be a Ti-rich layer (Fig. 8c). An increase in the intensity of calcium was also detected along the outer margin of this white line (Fig. 8c).

Evaluation of osteoconductivity

The affinity indices for all of the cements at six and 12 weeks, and the statistical comparisons, are shown in Fig. 9.

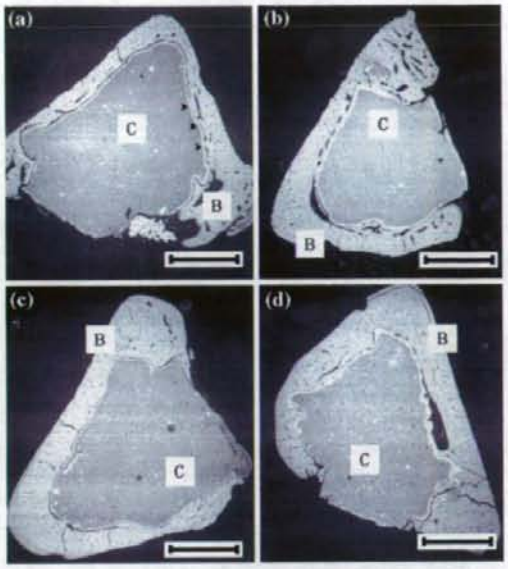

Fig. 6 Low magnification scanning electron micrographs of (**a**) ST2-50c and (**b**) ST2-56c in rat tibiae six weeks after implantation; (**c**) ST2-50c and (**d**) ST2-56c in rat tibiae 12 weeks after implantation. C, cement; B, bone; Arrowheads indicate the white line. Bar = 30 μm

Discussion

In preliminarily trials, it was attempted to prepare cements containing over 60 wt% micron-sized titania particles, but it was often difficult to effectively mix the powder and the liquid. Preliminary in vitro studies revealed that the apatite-forming ability of the composite cements increased with the content of titania particles. Because ST2-50c and ST2-56c were consistently made in a well-mixed form and were expected to have better osteoconductivity than ST2-40c, as judged from the in vitro studies, they were chosen for the animal study.

With the previously reported composite bone cement containing nanosized anatase-type titania particles, it was difficult to disperse the titania particles uniformly in the

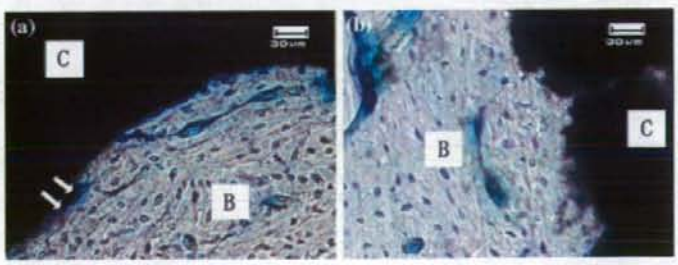

Fig. 5 Giemsa surface staining of (**a**) ST2-50c and (**b**) ST2-56c in rat tibiae 12 weeks after implantation. C, cement; B, bone; Arrows indicate intervening soft tissue. Bar = 30 μm